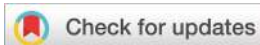




PAPER



Cite this: *Photochem. Photobiol. Sci.*, 2020, **19**, 207

Amplified luminescence quenching effect upon binding of nitrogen doped carbon nanodots to transition metal ions†

J. S. Anjali Devi,  R. S. Aparna, R. R. Anjana, N. S. Vijila, J. Jayakrishna and Sony George *

There is a significant drive to identify a unified emission mechanism hidden behind carbon nanodots (CDs) to attain reliable control over their photoluminescence properties. This issue is addressed here by investigating the fluorescence response of citric acid and urea-based nitrogen doped carbon nanodots (NCDs) towards transition metal ions in solutions of different polarities/viscosities/hydrogen bonding strengths. The photoluminescence from NCDs upon excitation at 400 nm is quenched by metal ions such as chromium(vi), ruthenium(iii) and iron(iii) in two different polar solvents, protic water and aprotic dimethylsulphoxide (DMSO). This amplified luminescence quenching in polar solutions showed significant static quenching contributions. The quenching phenomenon highly depends on the excitation wavelength and solvent environment. The fluorescence quenching sequence reveals that pyridinic nitrogen-bases have a dominant influence on J-like emissive aggregates of NCDs. Similarly, oxygen-containing functional groups play a significant role in constructing H-aggregates of NCDs. The most intense emission is contributed by the J-like assembly of H-aggregates.

Received 18th October 2019,
Accepted 24th December 2019

DOI: 10.1039/c9pp00420c

rsc.li/pps

1. Introduction

The use of carbon nanodots (CDs) for biological, optoelectronic and energy-related applications has matured rapidly over the past decade.¹ These luminescent materials are a boon to photonics research in the world because of their unique properties, namely room temperature phosphorescence, chirality and thermally activated delayed fluorescence.^{1–5} Biocompatible CDs synthesised through easy and cheap methods overcome many drawbacks of traditional organic dyes and semiconductor quantum dots.³ Unlike conventional fluorescent materials, the emission wavelength of CDs varies substantially with the excitation wavelength, while

it remains constant in some cases.⁶ Similarly, the sensitivity of CD fluorescence towards metal ions has undergone extensive investigation and various interpretations have been presented to accommodate diverse results.⁷ Gradual quenching of CD fluorescence in the presence of increasing metal ion concentration has been the most usual incident.^{8–10} In contrast, fluorescence enhancement in the presence of Ag⁺ has also been reported.¹¹ In addition, luminescent CDs are highly soluble in polar solvents like water and they exhibit solvatochromism.^{12–14} Consequently, the identification of a unanimous emission mechanism for CDs has continued to be a puzzle to date and this hinders reliable control over CD fluorescence in visible or near-infrared regions.

Copious efforts are made to identify the unified mechanism behind the anomalous fluorescence behaviour of CDs.¹⁵ Mostly, CDs are visualised as quasi-spherical carbon nanoparticles (~1–10 nm).¹ CDs feature an amorphous or nanocrystalline sp² carbon core implanted on the sp³ carbon backbone and a high density of polar functional groups on the surface imparting high hydrophilicity to CDs.¹⁶ The polar/hydrophilic functional groups (*e.g.*, polyphenol, alcohol, carboxyl, and carbonyl) on the surface of CDs vary with synthetic routes and precursors.¹ The fluorescence of CDs is ascribed to the luminescent electronic transition within the quantum-confined carbon core, surface defects or molecular fluorophores

Department of Chemistry, School of Physical and Mathematical Sciences, Research Centre, University of Kerala, Kariavattom Campus, Thiruvananthapuram-695581, Kerala, India. E-mail: emailtosony@gmail.com; Tel: +919446462933

†Electronic supplementary information (ESI) available: Synthesis of NCDs; experimental methods; ESI figures (Fig. S1–S16) illustrating characterisation using HRTEM, DLS technique, XPS, FTIR, steady state fluorescence, time resolved fluorescence and absorption spectroscopy; physical properties of solvents used in this study (Table S1); amplified quenching parameters of the previous conjugated polyelectrolytes and the present NCD system (Tables S2 and S3); time-resolved fluorescence decay parameters (Tables S4 and S5). See DOI: 10.1039/c9pp00420c

attached on the surface or in the interior of CDs.¹⁷ To our curiosity, several research reports since 2013 identified traces of molecular fluorophores (e.g., 2-pyridone derivatives such as citrazinic acid) in the reaction product obtained while following bottom-up synthetic routes to CDs (mostly, pyrolysis of molecular precursors), particularly in the case of citric acid derived nitrogen doped carbon nanodots (NCDs).^{2,18,19} Demchenko *et al.* proposed to extend Michael Kasha's 'J- and H-like aggregate model' for conventional molecular fluorophores to the photophysics of CDs in 2016 so that substantial attention is paid towards this concept in contemporary research on CDs.^{6,12,15,20,21} Kumbhakar's group tried to rationalise excitation dependent emission as well as the commonly observed disparity between absorption and excitation spectra of CDs using this J- and H-aggregate model.^{6,12} Our group has validated the emissive aggregate model by monitoring the excitation dependent emission of NCDs in different polar solvents.²¹ We found evidence of J-aggregates, H-aggregates, and JH-aggregate species of NCDs even in very dilute solutions. Still, several authors deviate from the emissive aggregate model of CDs.²² So a clear investigation of molecular fluorescence and aggregate behaviour hidden behind CDs is required.

Transition metal ions are reactive towards surface functional groups of CDs which is evident from numerous fluorescence quenching/enhancement studies on CDs.⁷ The emissive species and the quencher should be in close proximity to facilitate quenching.²³ Classically, fluorescence quenching is a widely adopted technique to analyse structural aspects of the fluorophore as well as energy/electron transfer interactions within fluorescent materials.^{23–26} A careful analysis of the quenching trend of NCDs gives an idea about the availability of emission centres to the quencher thereby providing a hint on the location of the emissive species within the NCD system.²³ A linear Stern–Völmer plot is an indication of a single class of emissive species whereas an upward curving Stern–Völmer plot represents combined static and dynamic quenching.^{23,24} Super quenching or amplified quenching is observed in the case of an exponential Stern–Völmer plot.^{23–26} Amplified quenching is strong evidence of aggregate formation, ion-pairing between the fluorophore and oppositely charged quencher and long distance migration of the exciton within the fluorescent material.^{24,26} Similarly, dynamic and static quenching can be differentiated by their varying dependency on viscosity.²³ Moreover, metal ions and solvent polarity/viscosity can be judiciously used for the modulation of J-/H-emissive aggregates of NCDs.^{20,27,28} In this direction, monitoring of transition metal ion-induced quenching of NCDs in two different solutions of different viscosities can definitely discriminate the J- and H-aggregate behaviour of NCDs in polar solvents.^{20,23,27} Consequently, a clear picture of the structural attributes of NCD aggregates can be obtained. Hence, we report the photophysical characterisation and transition metal ion-induced fluorescence quenching properties of hydrophilic citric acid derived NCDs in two polar solvents of varying viscosities – water and dimethylsulphoxide (DMSO).

2. Results and discussion

NCDs were synthesised by pyrolysis of citric acid and urea using a microwave-assisted hydrothermal method described elsewhere.²⁹ The detailed procedure is given in the ESI†. The synthesised NCDs were fully characterised by transmission electron microscopy (TEM), X-ray photoelectron spectroscopy (XPS), Fourier transform infrared (FTIR) spectroscopy and dynamic light scattering (DLS) techniques. TEM images of an aqueous dispersion of NCDs revealed the formation of spherical nanoparticles of around 3 to 5 nm (Fig. S1A in the ESI†). The size of nanoparticles increased to the 6 to 10 nm range upon dispersing NCDs in the DMSO medium (Fig. S1B in the ESI†). However, TEM images of NCDs in both solvents showed certain mesoscopic ribbon-like structures (Fig. S1C and D in the ESI†). These monolayer sheets resemble H-like aggregates as predicted by Demchenko *et al.*¹⁵ This observation is consistent with the findings of Kumbhakar's group who portrayed H-aggregates of CDs in their TEM images.^{6,12} XPS confirmed the presence of N-heterocycles (pyridine or pyrrole) along with ketone, alcohol, sp³ C–C bonds, amides/amines and carboxylate groups (Fig. S2 in the ESI†). The aqueous NCD samples displayed characteristic FTIR peaks at 1717.5 cm⁻¹ (COO–stretching), 1635.5 cm⁻¹ (C=O stretching of amides), 1475.3 cm⁻¹ (C=C stretching of aromatics), 1363.6 cm⁻¹ (O–H deformation of phenol) and 1080.4 cm⁻¹ (=C–O stretching of phenols) along with a broad band at approximately 3700–2800 cm⁻¹ (with peaks at 3490.9 cm⁻¹, 3364.2 cm⁻¹ and 3271.1 cm⁻¹ for N–H stretching of aromatic amines, O–H stretching of phenol/alcohol, and N–H stretching of amides, respectively) (see Fig. S3 in the ESI†). Many of these IR peaks with minor spectral shifts can be rediscovered in the IR spectrum of the NCD dispersion in the DMSO medium also. Thus, the FTIR spectrum and XPS data unanimously established the co-existence of heterocyclic aromatic units (such as citrazinic acid) with other polar functional groups on the NCD surface, an observation similar to previous reports by many research groups.^{12,19} However, these polar surface functional groups cumulatively contribute a neutral surface potential of +2.1 mV at pH 4 (Fig. S4A†). This neutral surface charge and polar functional groups can facilitate self-assembly (or aggregation) of NCDs in polar solvents like water which is expressed as the large hydrodynamic diameter of NCDs at all tested pH values (Fig. S4B–D†).¹²

The photophysical properties of the NCD dispersion in aqueous and DMSO medium were then thoroughly investigated using fluorescence and UV-visible absorption spectroscopy. As reported in the previous article elucidating excitation dependent emission of NCDs in aqueous solution,^{29,30} the maximum emission band of NCDs in DMSO medium shifts as the excitation wavelength changes (Fig. S5A and S5B†). This suggests superposition of various emissive species. The most intense emission is observed upon excitation at 400 nm in the DMSO medium. Then we keenly observed the fluorescence spectral shift by varying the NCD concentration. Fig. S5C† shows the luminescence spectra at different NCD

concentrations in DMSO with excitation at 400 nm. The fluorescence spectra demonstrate a slight increase in the intensity and a redshift in the emission maximum with an increase in the concentration up to $\sim 2.52 \text{ mg mL}^{-1}$ (Fig. S5C†). As the concentration increases further, the fluorescence intensity decreases with a redshift. Likewise, the fluorescence of the NCD dispersion in an aqueous medium with excitation at 400 nm follows a similar trend and attains the maximum intensity at a concentration of $\sim 3.76 \text{ mg mL}^{-1}$ (Fig. S5D†). Sequentially, we observed fluorescence excitation and fluorescence emission of NCDs in water ($\sim 6 \text{ mg mL}^{-1}$) and DMSO ($\sim 3 \text{ mg mL}^{-1}$) (see Fig. S6A†). The fluorescence excitation/emission spectra of NCD blueshift broaden and intensify as the solvent changes from water to DMSO. But the absorbance spectra (Fig. S6B†) undergo a blueshift of $\sim 23 \text{ nm}$ with a significant increase in absorbance with an increase in solvent polarity from DMSO to water (*i.e.*, NCDs exhibit negative solvatochromism).²³ Consequently, we monitored the time dependence of the fluorescence spectra of NCDs. Fig. S7† shows the fluorescence emission spectra of NCDs measured after different periods of storage in a sealed beaker at room temperature with sufficient exposure to room light and air. With the increase in the storage time, the fluorescence intensity of the aqueous NCD dispersion declines with a redshift. This implies an increased H-character (suppression of fluorescence with a redshift) of aqueous NCD samples on storage. In contrast, the NCD dispersion in the DMSO medium exhibits a slight blueshift in association with diminishing fluorescence intensity on storage. These features are hallmarks of emissive aggregates of NCDs in polar solvents like water or DMSO as reported previously.^{12,20} But these irregular fluorescence spectral shifts upon excitation at 400 nm cannot be explained by the involvement of simple H-aggregate or J-aggregates alone. Therefore, we suspected that a competition between J-favouring interactions and H-favouring interactions occurred inside the emissive aggregates of NCDs on changing the solvent polarity, concentration or storage time with excitation at 400 nm.²⁰ This predicts the existence of JH-aggregates of NCDs which are stimulated upon excitation at 400 nm.^{20,31}

In previous studies,^{7,30} we and others have shown that the addition of transition metal ions like Fe^{3+} to an aqueous NCD dispersion leads to aggregation and fluorescence quenching. To gain more insight into this phenomenon in NCDs, initial studies focus on the fluorescence spectral behaviour of NCDs upon the addition of prominent transition metal ions [Cr^{3+} , Cr^{6+} , Mn^{2+} , Fe^{2+} , Fe^{3+} , Ru^{3+} , Co^{2+} , Ni^{2+} , Cu^{2+} , Ag^+ , Zn^{2+} , Cd^{2+} , Hg^{2+} , and Pb^{2+}] in aqueous and DMSO solution under ambient oxygen conditions (Fig. 1). As expected, different metal ions vary considerably in their ability to quench NCD fluorescence. The role of dynamic and static quenching can be distinguished by a quantitative comparison of relative fluorescence quenching in two solvents of different viscosities.²³ Generally, a highly viscous medium (here, it is DMSO; see Table S1†) strengthens a weak ground state complex formed during static quenching. This effect is clear from the higher quenching efficiency of Cr^{3+} , Mn^{2+} , Fe^{2+} , Ni^{2+} , Cu^{2+} , Zn^{2+} , Cd^{2+} ,

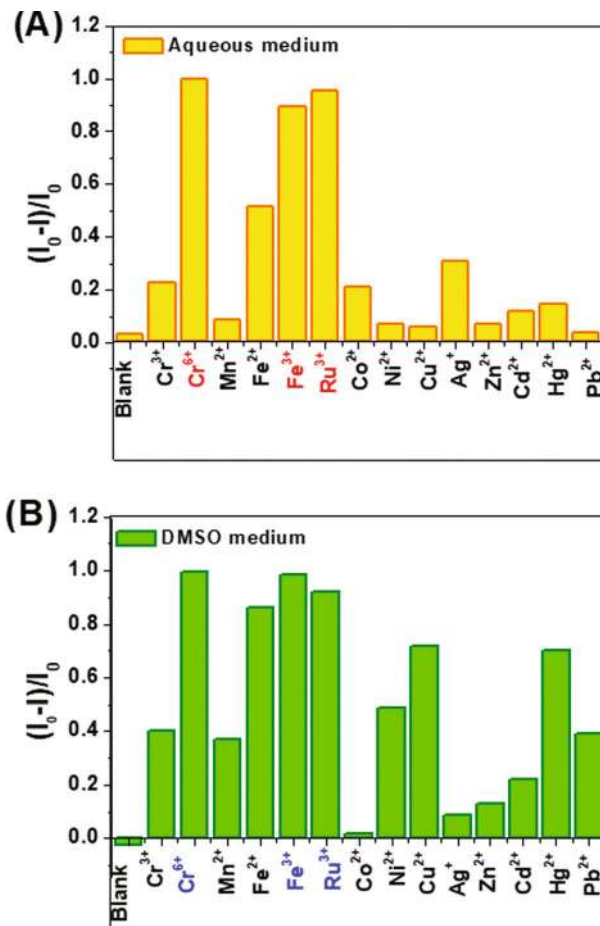


Fig. 1 The comparison of the fluorescence quenching effect on nitrogen doped carbon nanodots (NCDs) after the addition of different metal ions in: (A) aqueous solution and (B) DMSO solution. The concentration of metal ions except for Ru^{3+} in aqueous solution is $3225.8 \mu\text{M}$. The concentration of Ru^{3+} in aqueous solution is $1549.0 \mu\text{M}$. The concentration of metal ions except for Cr^{6+} and Ru^{3+} in the DMSO solution is $2597.4 \mu\text{M}$. The concentration of Cr^{6+} in the DMSO solution is $1315.7 \mu\text{M}$. The concentration of Ru^{3+} in the DMSO solution is $657.89 \mu\text{M}$.

Pb^{2+} and Hg^{2+} in DMSO solution than in aqueous solution. In contrast, dynamic quenching due to weak quenchers may be hindered in solvents of higher viscosity (*i.e.*, DMSO). This phenomenon is manifested by weak quenching efficiency of Ag^+ and Co^{2+} (*i.e.*, quenching by the external heavy atom effect) in the DMSO medium as compared to the aqueous medium. Herein, we focus mostly on the fluorescence quenching experiments with Cr^{6+} , Fe^{3+} , and Ru^{3+} , which led to the most pronounced quenching.

Next, Stern–Völmer fluorescence quenching experiments were carried out on NCDs in aqueous solution (pH 4) using Cr^{6+} , Fe^{3+} , and Ru^{3+} as quenchers (excitation wavelength = 400 nm). The NCD concentration was 6 mg mL^{-1} in water. The aqueous NCD dispersion emits at around 491 nm upon excitation at 400 nm. As shown in Fig. 2, the fluorescence intensity decreased in the sequence of $\text{Ru}^{3+} > \text{Cr}^{6+} > \text{Fe}^{3+}$. Unlike other

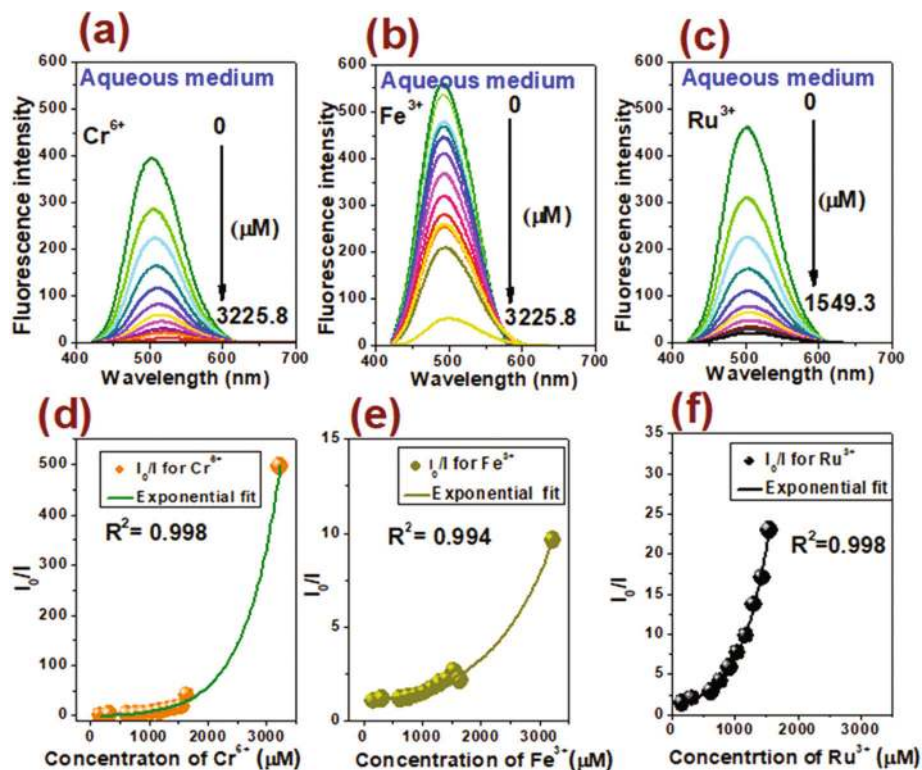
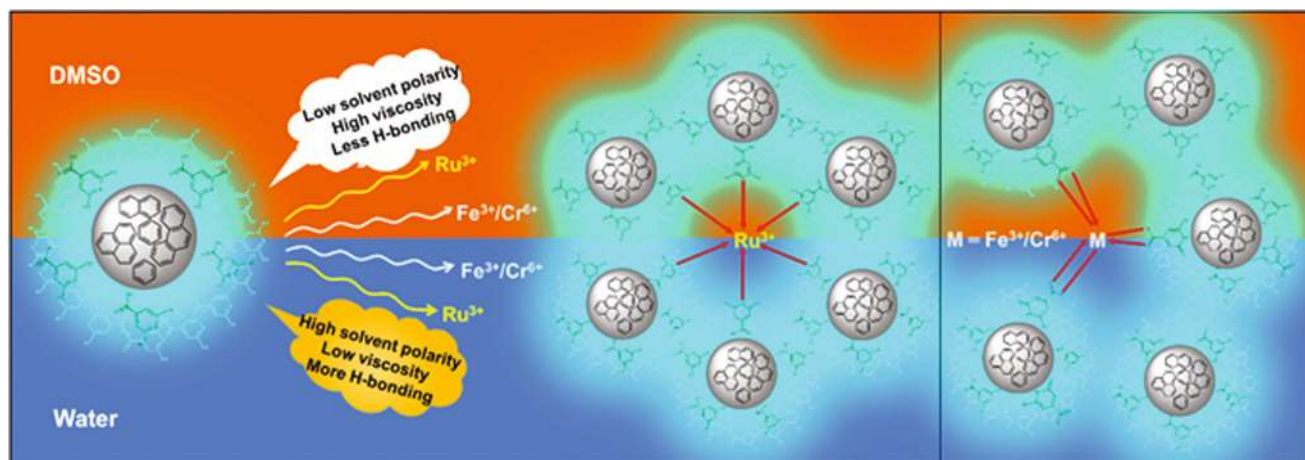


Fig. 2 Fluorescence emission spectra of the NCD (6 mg mL⁻¹) aqueous dispersion (pH 4) in the presence of different concentrations of: (a) Cr⁶⁺ [top to bottom: 0, 163.9, 322.6, 625.0, 769.2, 909.1, 1044.8, 1176.5, 1304.4, 1428.6, 1549.3, 1639.3 and 3225.8 μM], (b) Fe³⁺ [top to bottom: 0, 163.9, 322.6, 625.0, 769.2, 909.1, 1044.8, 1176.5, 1304.4, 1428.6, 1549.3, 1639.3 and 3225.8 μM] and (c) Ru³⁺ [top to bottom: 0, 163.9, 322.6, 625.0, 769.2, 909.1, 1044.8, 1176.5, 1304.4, 1428.6 and 1549.3 μM]. Stern-Völmer plots of NCD fluorescence quenched by metal ions in water: (d) Cr⁶⁺ {I₀/I = -4.18 + 2.03 exp(1.70[Cr⁶⁺]/1000)}, (e) Fe³⁺ {I₀/I = 0.52 + 0.39 exp(0.97[Fe³⁺]/1000)} and (f) Ru³⁺ {I₀/I = 0.54 + 0.65 exp(2.30[Ru³⁺]/1000)}. Excitation: 400 nm.

metal ions, Ru³⁺ induced quenching retains the symmetrical Gaussian shape of the photoluminescence spectrum even at maximum quenching. The higher quenching effect of Ru³⁺ can be correlated to the higher affinity of Ru³⁺ to N-containing bases like pyridine [hard and soft (Lewis) acid and base concept]. Upon analysing this sequence, we realized that Cr⁶⁺ and Fe³⁺ are more sensitive towards oxygen-containing functional groups than nitrogen bases (see Scheme 1). In addition, Cr⁶⁺ possesses a higher positive charge density than Fe³⁺. The observed quenching trend suggests that among oxygen and nitrogen containing functional groups, nitrogen containing groups like pyridine or pyrrole have predominant control over emissive states upon excitation at 400 nm. The lower panel of Fig. 2 displays the corresponding upward curving Stern-Völmer plots (plot of I₀/I versus concentration of the quencher) for aqueous NCD solution with Ru³⁺, Cr⁶⁺, and Fe³⁺. Consequently, we calculate the Stern-Völmer quenching constant (K_{SV}) and [Q]₅₀ values from the linear region of the plot (*i.e.*, at a lower quencher concentration) (see Fig. S8 and Table S2†). Note that a linear Stern-Völmer plot gives an intercept of one on the y-axis and the slope is equal to K_{SV}. The inverse of K_{SV} (*i.e.*, K_{SV}⁻¹) is the quencher concentration at I₀/I = 2 or 50% of fluorescence intensity gets quenched.²³ Fluorescence quenching studies on NCDs with selected metal cations give

K_{SV} values of 3000 M⁻¹ {Ru³⁺}, 2090 M⁻¹ {Cr⁶⁺} and 280 M⁻¹ {Fe³⁺}, consistent with amplified quenching (Tables S2 and S3†).^{24,32} The corresponding [Q]₅₀ values are 333.3 μM, 478.5 μM, and 3571.4 μM, respectively. These results suggest that NCDs form transition metal ion-induced aggregates during the quenching process in an aqueous medium.^{32,33}

Out of curiosity, we monitored Stern-Völmer quenching experiments using selected metal ions [*i.e.*, Cr⁶⁺, Fe³⁺ and Ru³⁺] with NCDs in DMSO solution under ambient oxygen conditions. We observed that the hydrogen bonding ability and viscosity of DMSO are extremely different from those of water so that DMSO will provide a different environment for studies on metal ion-induced quenching.¹³ Fig. 3 summarises the data of fluorimetric titration of metal ions in DMSO medium. The fluorescence intensity (λ_{max} = 481 nm) of the NCD dispersion (~3 mg mL⁻¹) in DMSO decreases in the sequence of Cr⁶⁺ > Ru³⁺ > Fe³⁺. This trend is somewhat in the order of positive charge density on the metal ions [*i.e.*, Cr⁶⁺ > Fe³⁺ > Ru³⁺].³³ The higher quenching effect of Ru³⁺ as compared to Fe³⁺ can be substantiated by the higher affinity of Ru³⁺ towards N-nucleophiles like pyridine than Fe³⁺ [hard and soft (Lewis) acid and base concept]. The lower panel of Fig. 3 depicts the corresponding exponential Stern-Völmer plots demonstrating an amplified quenching phenomenon. The calculated K_{SV}



Scheme 1 Scheme illustrating fluorescence quenching of nitrogen doped carbon nanodots by transition metal ions in DMSO (top panel) and aqueous solutions (bottom panel). The quenching effect of Ru^{3+} occurs through higher affinity of Ru^{3+} to nitrogen containing bases like pyridine. Fe^{3+} and Cr^{6+} ions interact mostly with oxygen rich functional groups like carboxyl and phenolic groups.

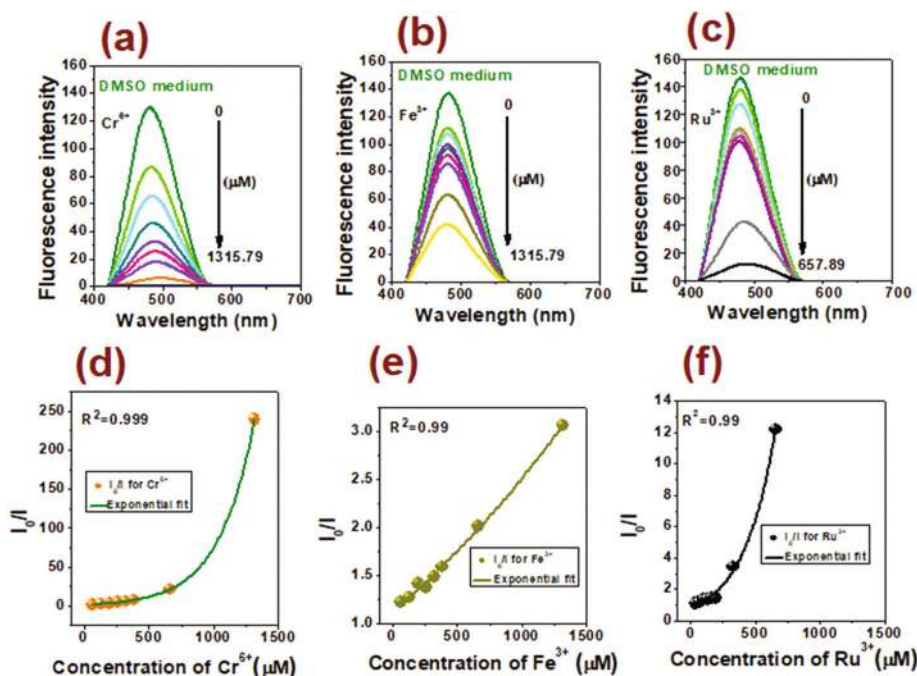


Fig. 3 Fluorescence emission spectra of the NCD (3 mg mL^{-1}) dispersion in DMSO in the presence of different concentrations of: (a) Cr^{6+} [top to bottom: 0, 66.2, 131.6, 196.1, 259.7, 322.6, 384.6, 662.5 and $1315.8 \mu\text{M}$], (b) Fe^{3+} [top to bottom: 0, 66.2, 131.6, 196.1, 259.7, 322.6, 384.6, 662.5 and $1315.8 \mu\text{M}$] and (c) Ru^{3+} [top to bottom: 0, 33.1, 65.8, 98.0, 129.9, 161.3, 192.3, 231.1 and $657.9 \mu\text{M}$]. Stern–Völmer plots of NCD (3 mg mL^{-1}) fluorescence quenched by metal ions in DMSO: (d) Cr^{6+} $\{I_0/I\} = -1.09 + 1.97 \exp(3.70[\text{Cr}^{6+}]/1000)$, (e) Fe^{3+} $\{I_0/I\} = -2.03 + 3.16 \exp(0.36[\text{Fe}^{3+}]/1000)$ and (f) Ru^{3+} $\{I_0/I\} = -0.03 + 0.84 \exp(4.10[\text{Ru}^{3+}]/1000)$. Excitation: 400 nm.

values are $10\,000 \text{ M}^{-1}$ $\{\text{Cr}^{6+}\}$, 2410 M^{-1} $\{\text{Ru}^{3+}\}$ and 1480 M^{-1} $\{\text{Fe}^{3+}\}$. The corresponding $[Q]_{50}$ values are $100 \mu\text{M}$, $414.9 \mu\text{M}$, and $675.7 \mu\text{M}$, respectively (see Fig. S9 and Table S2†).

The fluorescence quenching in NCDs can be caused by Förster resonance energy transfer (FRET), inner filter effect (IFE), photoinduced electron transfer (PET), and changes in absorption (spectral bleaching), aggregation and quenching *via* a static or dynamic mechanism.^{23,34–36} Prior to further

studies, it is worth discussing the probability of each of these alternatives.

Since the overlap between the absorption spectrum of the selected metal ion quenchers and the emission spectrum of NCDs is not so significant, the possibility of the FRET mechanism can be side-lined (Fig. S10 and S11†).²³ However, the absorption spectrum of the major quencher ions overlaps with the excitation spectrum of NCDs which suggests that IFE can

play a role in quenching.^{30,34} Consequently, we tried to compute the possible energy transfer rate (k_{ET}) between the quenchers and NCDs by the equation:²⁶ $k_{ET} = \frac{1}{\langle\tau\rangle} - \frac{1}{\langle\tau_0\rangle}$ (Table S4†) ($\langle\tau\rangle$ and $\langle\tau_0\rangle$ are the average fluorescence lifetimes of NCDs with and without metal ion quenchers). It is observed that energy transfer has a very minor effect.

If oxidative PET occurs, an electron from the highest occupied molecular orbital of a NCD gets transferred to the lowest unoccupied molecular orbital of metal ions. In this way, metal ions with the highest positive reduction potential should be the best quencher.³⁶ Since the observed order of metal ion-induced quenching does not obey the sequence of the standard reduction potential ($Ru^{3+} = +0.68$ V; $Cr_2O_7^{2-} = +1.33$ V and $Fe^{3+} = +0.77$ V), fluorescence quenching is not solely because of oxidative PET. According to previous reports, the electron transfer reaction between a fluorescent single-walled carbon nanotube and a redox quencher can be diagnosed by monitoring changes in the absorption properties of the carbon nanomaterial.³⁵ As seen in Fig. 4, there is a significant decrease in absorbance in the absorbance spectra accompanied by Ru^{3+} induced quenching in aqueous solution and Cr^{6+} induced quenching in the DMSO solution. The reaction of NCDs with other metal ions in this study resulted in changes in the absorption properties of NCDs but with differing trends and effectiveness. To our surprise, the addition of Fe^{3+} and Cr^{6+} causes a hyperchromic shift in the absorbance spectra of NCDs in aqueous solution. This Fe^{3+} induced hyperchromic effect on the absorption band of NCDs becomes much stronger in the DMSO solution. These changes in the absorbance spectrum along with quenching suggest that static quenching or ground state complex formation is the

major reason for the quenching process in the present case.³⁰ Moreover, XPS of NCDs with Cr^{6+} show no Cr^{6+} peaks, but Cr^{3+} peaks are very clearly visible (Fig. S12†). XPS analysis reveals that Cr^{3+} is connected to NCDs through Cr-carbonate, Cr-carbide and Cr-nitride bonds. The elemental ratio is C:N:O:Cr = 66.5:9.1:24.3:0.1 (Fig. S13†). These records suspect that the electron transfer process competes with ground-state complex formation (static quenching and aggregation). Besides, the upward-curving nature of the exponential Stern-Völmer plot proves this competitive nature such that the system never attains maximum quenching even at higher quencher concentrations.³⁷

The significant interest of this work is to examine the amplified quenching phenomenon in NCDs. The tested quenchers are cations and they are expected to interact with polar surface groups of NCDs *via* ion pairing, which is an important aspect of the amplified quenching mechanism.^{24,37} Also, Ru^{3+} , Cr^{6+} and Fe^{3+} can bind with multiple carboxylate, hydroxyl or nitrogen-containing functional groups³³ and thus, can facilitate bridging between adjacent NCD entities. From these large K_{SV} values and nanosecond lifetime decay profiles (Fig. S14†), it is evident that quenching occurs *via* a static mechanism, involving ion-pair complexes between polar functional groups of NCDs and cationic quenchers. The Stern-Völmer quenching plots with substantial upward curvature has been correlated to quencher induced NCD aggregation.³⁷

The excitation profile of NCDs is extremely different from their absorbance spectrum. Sequentially, fluorescent decay traces of NCDs in aqueous and DMSO medium at different excitation wavelengths are observed to be considerably different (Fig. S14 and S15†). Quenching studies carried out using time-resolved emission upon excitation corresponding to the absorp-

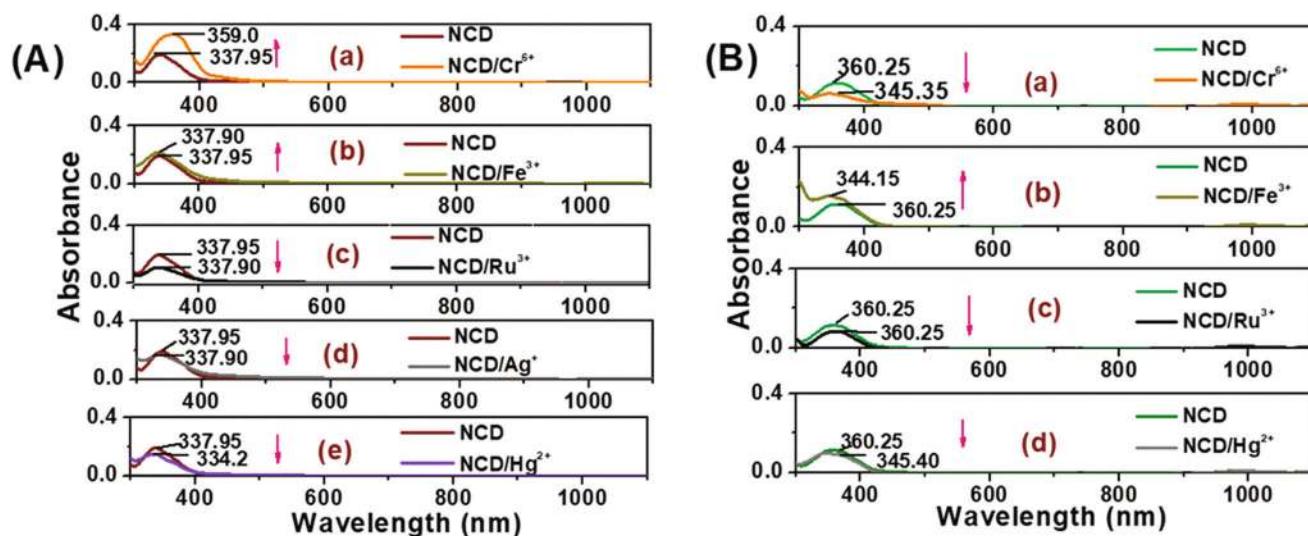


Fig. 4 (A) The absorbance spectra of the bare NCD suspension (brown line) and NCD suspension after addition of transition metal ions in water: (a) Cr^{6+} (orange line), (b) Fe^{3+} (dark yellow line), (c) Ru^{3+} (black line), (d) Ag^+ (grey line), and (e) Hg^{2+} (violet line). The concentration of all metal ions except Ru^{3+} is 1639.3 μM . The concentration of Ru^{3+} is 819.65 μM . (B) The absorbance spectra of the bare NCD suspension (green line) and NCD suspension after addition of transition metal ions in DMSO: (a) Cr^{6+} (orange line), (b) Fe^{3+} (dark yellow line), (c) Ru^{3+} (black line) and (d) Hg^{2+} (grey line). The concentration of all metal ions except Ru^{3+} is 1639.3 μM . The concentration of Ru^{3+} is 819.65 μM .

tion maximum reveal slight variations in fluorescence lifetime data and null energy transfer during the quenching process (Tables S4 and S5[†]). This result predicts that the species that emit at each excitation wavelength possesses different optical properties. However, the decay traces of NCDs are tri-exponential at all tested excitation wavelengths. Therefore, we assigned a high energy weak excitation band to H-aggregates and a low energy intense excitation band to JH-aggregates.^{12,21} The absorbance band at around 337 nm (in water) or 360 nm (in DMSO) can be correlated to J-aggregates. Sequentially we carry out excitation dependent quenching studies on NCDs.

It has been reported previously that both weak high energy excitation bands and intense low energy excitation bands of NCDs are accessible to quenchers.¹² In this direction, we examined the excitation spectrum of NCDs before and after the addition of metal ion quenchers (Fig. 5 and 6). The spectral evidence indicates that metal ion quenchers like Cr^{6+} and Fe^{3+} have a much pronounced relative quenching (I_0/I) effect on weakly emissive high energy excitation bands than on intense low energy bands. This excitation wavelength depen-

dency on quenching indicates the inhomogeneous nature of NCD fluorescence which in turn points to the distribution of different emissive species in the ensemble used for fluorescence spectroscopy.³⁸ A close look at fluorescence quenching at different excitation wavelengths also reveals the presence of different emissive species since the selected set of metal ions follow different trends of fluorescence quenching at different excitation wavelengths (Fig. S16,[†] Table 1). For instance, Ru^{3+} is sensitive to N-bases like pyridine and exhibits a significant quenching effect on the excitation of J-aggregates (*i.e.*, 340 nm). This suggests the involvement of N-bases in the formation of J-like emissive aggregates of NCDs. Furthermore, oxygen-sensitive Cr^{6+} or Fe^{3+} lead to pronounced quenching upon excitation of H-aggregates (*i.e.*, at 300 nm). This indicates the major contribution of oxygen-containing functional groups for the construction of H-like emissive aggregates of NCDs. Thus, conventional theories correlating fluorescence emission of CDs with the luminescent electronic transition of the quantum sized graphitic core or surface defects is not appropriate to substantiate these results.

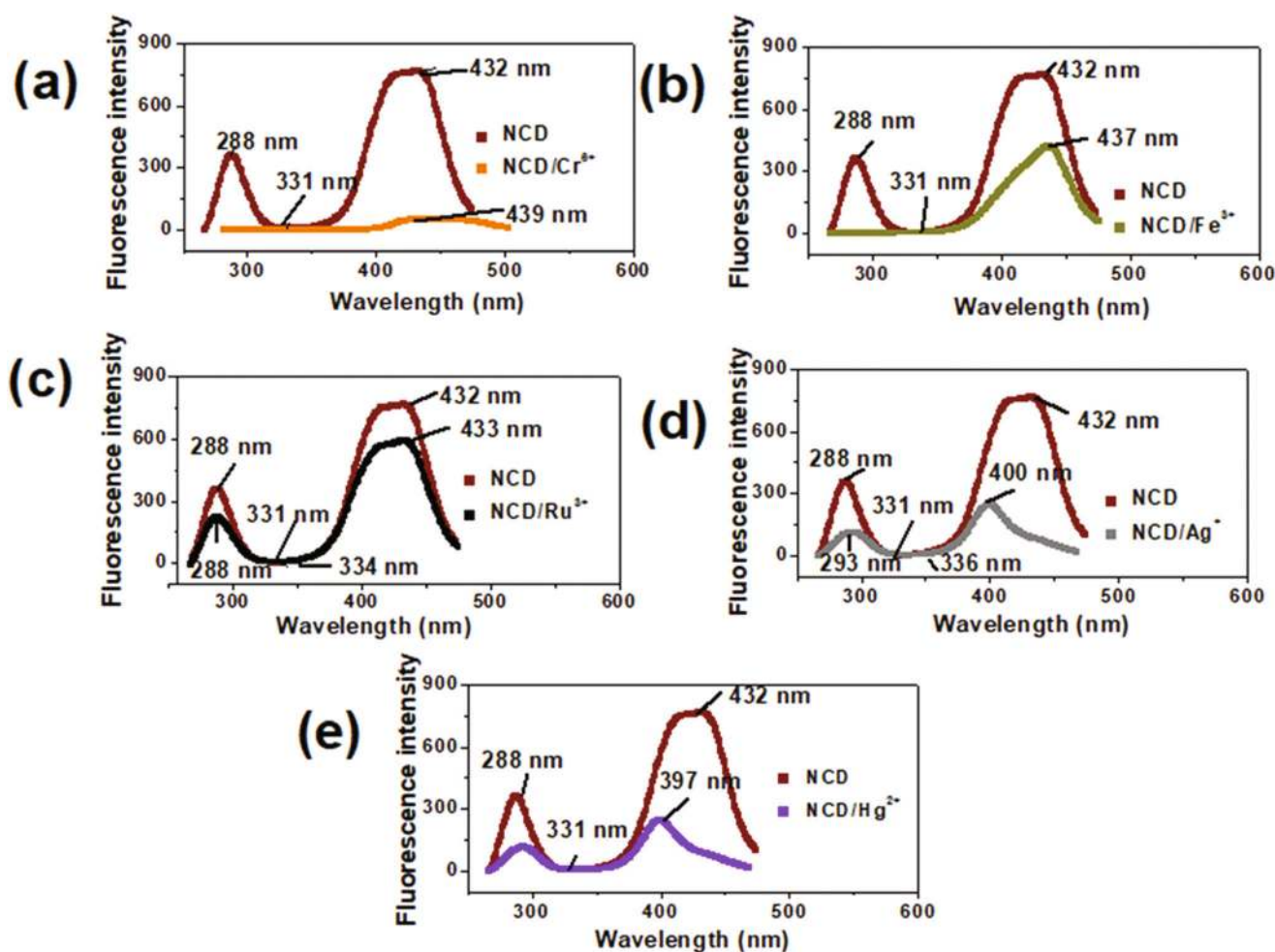


Fig. 5 The excitation spectra of the NCD dispersion in water before ($\lambda_{\text{em}} = 491$ nm) and after the addition of metal ion quenchers. The metal ions are: (a) Cr^{6+} ($\lambda_{\text{em}} = 522$ nm), (b) Fe^{3+} ($\lambda_{\text{em}} = 496$ nm), (c) Ru^{3+} ($\lambda_{\text{em}} = 494$ nm), (d) Ag^+ ($\lambda_{\text{em}} = 488$ nm) and (e) Hg^{2+} ($\lambda_{\text{em}} = 495$ nm). The concentration of Cr^{6+} , Fe^{3+} , Ag^+ , and Hg^{2+} are ~ 1600 μM . The concentration of Ru^{3+} is ~ 160 μM .

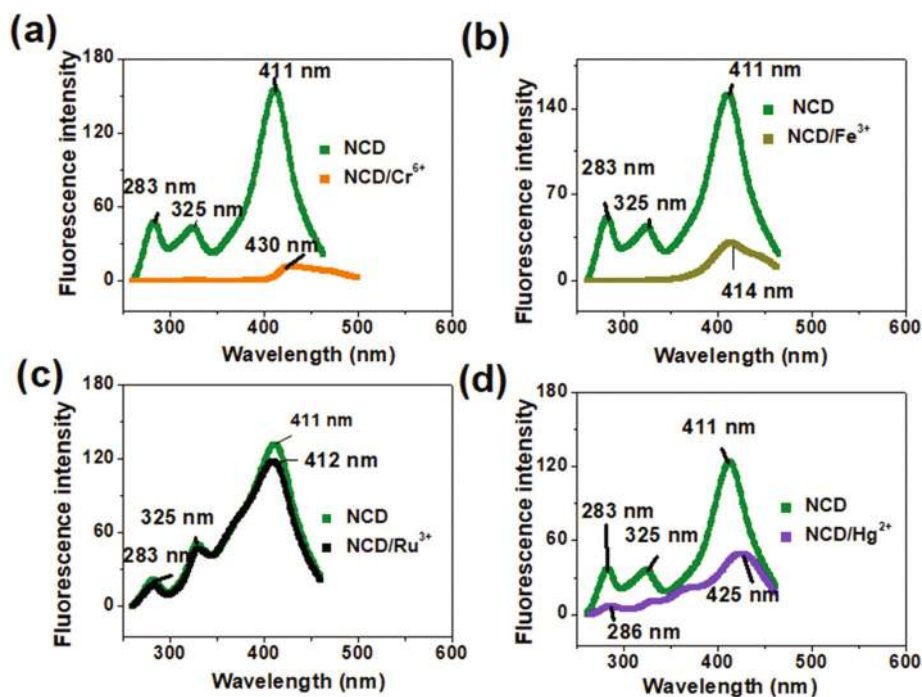


Fig. 6 The excitation spectra of the NCD dispersion in DMSO before ($\lambda_{em} = 481$ nm) and after the addition of metal ion quenchers. The metal ions are: (a) Cr^{6+} ($\lambda_{em} = 480$ nm), (b) Fe^{3+} ($\lambda_{em} = 479$ nm), (c) Ru^{3+} ($\lambda_{em} = 494$ nm) and (d) Hg^{2+} ($\lambda_{em} = 495$ nm). The concentration of Cr^{6+} , Fe^{3+} , and Hg^{2+} are ~ 1600 μM . The concentration of Ru^{3+} is ~ 160 μM .

Table 1 Fluorescence quenching of NCDs by metal ions [Cr^{6+} , Fe^{3+} and Ru^{3+}] in aqueous and DMSO solution at different excitation wavelengths ($\lambda_{ex} = 300, 340, 400$ and 480 nm). The concentrations of Fe^{3+} and Cr^{6+} are ~ 1600 μM . The concentration of Ru^{3+} is ~ 160 μM

Sample	Solvent	I_0/I			
		$\lambda_{ex} = 300$ nm	$\lambda_{ex} = 340$ nm	$\lambda_{ex} = 400$ nm	$\lambda_{ex} = 480$ nm
NCD/ Cr^{6+}	Water	126.95	11.82	77.11	3.10
	DMSO	113.56	40.25	139.24	1.63
NCD/ Fe^{3+}	Water	29.79	2.54	2.51	0.53
	DMSO	683.34	25.96	5.51	2.39
NCD/ Ru^{3+}	Water	1.44	1.95	1.27	1.20
	DMSO	1.25	1.01	1.06	1.08

Importantly, amplified quenching is a very common feature of conjugated polyelectrolyte-ionic quencher systems (see Table S3[†]).²⁴ So, there could be phenomenological similarities between the luminescence emission mechanism in conjugated polyelectrolyte and NCDs. Interestingly, many conjugated polymers self-assembled in suitable solvents and exhibited both J- or H-aggregate characters.^{31,39,40} Consequently, a transition metal ion controlled amplified quenching phenomenon in NCDs reveals the J-, H- and JH-aggregate structure of NCDs. Thus, NCD synthesis can be visualised as the spontaneous aggregation of fluorophores and carbonisation of these aggregates so that these emissive aggregates allow exciton migration over the entire particle leading to its characteristic emission by electron-hole pair recombination.

3. Conclusions

In conclusion, amplified fluorescence quenching of citric acid derived NCDs with a series of multivalent transition metal ions in two polar solvents of different polarities/viscosities/hydrogen bonding strengths is investigated. This amplified quenching phenomenon correlates the luminescence emission mechanism in NCDs with that of certain conjugated polyelectrolytes. More specifically, the transition metal ion controlled amplified quenching phenomenon in NCDs substantiates the J-, H- and JH-emissive aggregate structure of a NCD. Also, NCD synthesis can be visualised as the spontaneous aggregation of fluorophores and carbonisation of these aggregates to carbonised nanoparticles having sufficient surface-exposed fluorophores. The as-constructed nanoparticles self-assembled in polar solvents into typical J-, H- or JH-aggregates and allowed exciton migration over the entire emissive aggregate leading to its characteristic emission by electron-hole pair recombination. The amplified quenching process involves the initial ion pairing of polar surface groups of NCDs with metal cations, and then quencher induced aggregation and final critical changes in the original self-assembly pattern of J-, H- or JH-emissive aggregates of NCDs in polar solvents. This process facilitates much larger non-emissive aggregate formation and long distance diffusion of the photoexcited electrons within these non-emissive aggregates of NCDs. Moreover, it is observed that weakly emissive high energy excitation bands are more susceptible to oxygen-sensitive metal ion quenchers than highly intense low energy excitation bands. Similarly, different

quenching sequences for the selected set of metal ions are observed at different excitation wavelengths. Ru³⁺ is more sensitive to N-bases like pyridine and exhibits a significant quenching effect upon excitation of J-like emissive aggregates (*i.e.*, 340 nm). This suggests the involvement of N-bases in the formation of J-like emissive aggregates of NCDs. Furthermore, oxygen sensitive Cr⁶⁺ or Fe³⁺ leads to pronounced quenching upon excitation of H-aggregates (*i.e.*, at 300 nm). This indicates the major contribution of oxygen-containing functional groups towards the construction of H-like emissive aggregates of NCDs. Besides, a competition between J-favouring interactions and H-favouring interactions occurred inside the emissive aggregates of NCDs upon changing the solvent polarity, concentration or storage time while being excited at 400 nm. This predicts the existence of JH-aggregates of NCDs which are stimulated upon excitation at 400 nm. These results cumulatively indicate the existence of J-, H- and JH-like emissive aggregates of NCDs with an extremely different chemical structure.

Conflicts of interest

The author(s) declare no competing financial interest.

Acknowledgements

The authors gratefully acknowledge the encouragement, generous support and instrumental facilities from the Professor & Head of the host institution, Department of Chemistry, the University of Kerala, India. The authors thank CLIF-SICC, Kariavattom Campus, the University of Kerala for helping with the XPS analysis. The HR-TEM facility of DST-SAIF, STIC, Kochi, India is being acknowledged. The authors express sincere thanks to SAIF, MGU, Kottayam, India for TCSPC measurements upon excitation at 330 nm. J. S. Anjali Devi acknowledges the Department of Science and Technology, Government of India, for her DST-INSPIRE fellowship (IF 150393).

References

- X. Li, M. Rui, J. Song, Z. Shen and H. Zeng, Carbon and Graphene Quantum Dots for Optoelectronic and Energy Devices: A Review, *Adv. Funct. Mater.*, 2015, **25**, 4929–4947.
- Y. Xiong, J. Schneider, E. V. Ushakova and A. L. Rogach, Influence of molecular fluorophores on the research field of chemically synthesized carbon dots, *Nano Today*, 2018, **23**, 124–139.
- D. C. Green, M. A. Holden, M. A. Levenstein, S. Zhang, B. R. G. Johnson, J. Gala de Pablo, A. Ward, S. W. Botchway and F. C. Meldrum, Controlling the fluorescence and room-temperature phosphorescence behaviour of carbon nanodots with inorganic crystalline nanocomposites, *Nat. Commun.*, 2019, **10**, 206.
- L. Dordević, F. Arcudi, A. D'Urso, M. Cacioppo, N. Micali, T. Bürgi, R. Purrello and M. Prato, Design principles of chiral carbon nanodots help convey chirality from molecular to nanoscale level, *Nat. Commun.*, 2018, **9**, 3442.
- J. Liu, N. Wang, Y. Yu, Y. Yan, H. Zhang, J. Li and J. Yu, Carbon dots in zeolites: A new class of thermally activated delayed fluorescence materials with ultralong lifetimes, *Sci. Adv.*, 2017, **3**, e1603171.
- A. Sharma, T. Gadly, A. Gupta, A. Ballal, S. K. Ghosh and M. Kumbhakar, Origin of Excitation Dependent Fluorescence in Carbon Nanodots, *J. Phys. Chem. Lett.*, 2016, **7**, 3695–3702.
- Y. Dong, J. Cai, X. You and Y. Chi, Sensing applications of luminescent carbon based dots, *Analyst*, 2015, **140**, 7468–7486.
- S. Zhu, Q. Meng, L. Wang, J. Zhang, Y. Song, H. Jin, K. Zhang, H. Sun, H. Wang and B. Yang, Highly Photoluminescent Carbon Dots for Multicolor Patterning, Sensors, and Bioimaging, *Angew. Chem., Int. Ed.*, 2013, **52**, 3953–3957.
- M. J. Krysmann, A. Kellarakis, P. Dallas and E. P. Giannelis, Formation Mechanism of Carbogenic Nanoparticles with Dual Photoluminescence Emission, *J. Am. Chem. Soc.*, 2012, **134**, 747–750.
- S. Dutta Choudhury, J. M. Chethodil, P. M. Gharat, P. K. Praseetha and H. Pal, pH-Elicited Luminescence Functionalities of Carbon Dots: Mechanistic Insights, *J. Phys. Chem. Lett.*, 2017, **8**, 1389–1395.
- Z. Qian, J. Ma, X. Shan, H. Feng, L. Shao and J. Chen, Highly Luminescent N-Doped Carbon Quantum Dots as an Effective Multifunctional Fluorescence Sensing Platform, *Chem. – Eur. J.*, 2014, **20**, 2254–2263.
- A. Sharma, T. Gadly, S. Neogy, S. K. Ghosh and M. Kumbhakar, Molecular Origin and Self-Assembly of Fluorescent Carbon Nanodots in Polar Solvents, *J. Phys. Chem. Lett.*, 2017, **8**, 1044–1052.
- A. Sciortino, E. Marino, B. van Dam, P. Schall, M. Cannas and F. Messina, Solvatochromism Unravels the Emission Mechanism of Carbon Nanodots, *J. Phys. Chem. Lett.*, 2016, **7**, 3419–3423.
- S. Mukherjee, E. Prasad and A. Chadha, H-Bonding controls the emission properties of functionalized carbon nano-dots, *Phys. Chem. Chem. Phys.*, 2017, **19**, 7288–7296.
- A. P. Demchenko and M. O. Dekaliuk, The origin of emissive states of carbon nanoparticles derived from ensemble-averaged and single-molecular studies, *Nanoscale*, 2016, **8**, 14057–14069.
- S. Y. Lim, W. Shen and Z. Gao, Carbon quantum dots and their applications, *Chem. Soc. Rev.*, 2015, **44**, 362–381.
- Q. Xu, T. Kuang, Y. Liu, L. Cai, X. Peng, T. Sreenivasan Sreeprasad, P. Zhao, Z. Yu and N. Li, Heteroatom-doped carbon dots: synthesis, characterization, properties, photoluminescence mechanism and biological applications, *J. Mater. Chem. B*, 2016, **4**, 7204–7219.
- W. Kasprzyk, S. Bednarz and D. Bogdał, Luminescence phenomena of biodegradable photoluminescent poly(diols citrates), *Chem. Commun.*, 2013, **49**, 6445.

- 19 W. Kasprzyk, T. Świergosz, S. Bednarz, K. Walas, N. V. Bashmakova and D. Bogdał, Luminescence phenomena of carbon dots derived from citric acid and urea—a molecular insight, *Nanoscale*, 2018, **10**, 13889–13894.
- 20 N. J. Hestand and F. C. Spano, Expanded Theory of H- and J-Molecular Aggregates: The Effects of Vibronic Coupling and Intermolecular Charge Transfer, *Chem. Rev.*, 2018, **118**, 7069–7163.
- 21 J. S. Anjali Devi, R. S. Aparna, R. R. Anjana, J. Nebu, S. M. Anju and S. George, Solvent Effects: A Signature of J- and H-Aggregate of Carbon Nanodots in Polar Solvents, *J. Phys. Chem. A*, 2019, **123**, 7420–7429.
- 22 N. Basu and D. Mandal, Solvatochromic Response of Carbon Dots: Evidence of Solvent Interaction with Different Types of Emission Centers, *J. Phys. Chem. C*, 2018, **122**, 18732–18741.
- 23 J. R. Lakowicz, *Principles of Fluorescence Spectroscopy*, Springer US, 2013.
- 24 C. Tan, E. Atas, J. G. Müller, M. R. Pinto, V. D. Kleiman and K. S. Schanze, Amplified quenching of a conjugated polyelectrolyte by cyanine dyes, *J. Am. Chem. Soc.*, 2004, **126**, 13685–13694.
- 25 C. Tan, M. R. Pinto and K. S. Schanze, Photophysics, aggregation and amplified quenching of a water-soluble poly(phenylene ethynylene), *Chem. Commun.*, 2002, 446–447.
- 26 L. Cao, Z. Lin, W. Shi, Z. Wang, C. Zhang, X. Hu, C. Wang and W. Lin, Exciton Migration and Amplified Quenching on Two-Dimensional Metal–Organic Layers, *J. Am. Chem. Soc.*, 2017, **139**, 7020–7029.
- 27 N. Goswami, Q. Yao, Z. Luo, J. Li, T. Chen and J. Xie, Luminescent Metal Nanoclusters with Aggregation-Induced Emission, *J. Phys. Chem. Lett.*, 2016, **7**, 962–975.
- 28 Z. Luo, X. Yuan, Y. Yu, Q. Zhang, D. T. Leong, J. Y. Lee and J. Xie, From Aggregation-Induced Emission of Au(I)–Thiolate Complexes to Ultrabright Au(0)@Au(I)–Thiolate Core–Shell Nanoclusters, *J. Am. Chem. Soc.*, 2012, **134**, 16662–16670.
- 29 S. Qu, X. Wang, Q. Lu, X. Liu and L. Wang, A Biocompatible Fluorescent Ink Based on Water-Soluble Luminescent Carbon Nanodots, *Angew. Chem., Int. Ed.*, 2012, **51**, 12215–12218.
- 30 J. S. A. Devi, R. S. Aparna, B. Aswathy, J. Nebu, A. O. Aswathy and S. George, Understanding the Citric Acid-Urea Co-Directed Microwave Assisted Synthesis and Ferric Ion Modulation of Fluorescent Nitrogen Doped Carbon Dots: A Turn On Assay for Ascorbic Acid, *ChemistrySelect*, 2019, **4**, 816–824.
- 31 N. J. Hestand and F. C. Spano, Molecular Aggregate Photophysics beyond the Kasha Model: Novel Design Principles for Organic Materials, *Acc. Chem. Res.*, 2017, **50**, 341–350.
- 32 F. Feng, J. Yang, D. Xie, T. D. McCarley and K. S. Schanze, Remarkable Photophysics and Amplified Quenching of Conjugated Polyelectrolyte Oligomers, *J. Phys. Chem. Lett.*, 2013, **4**, 1410–1414.
- 33 J. Yang, D. Wu, D. Xie, F. Feng and K. S. Schanze, Ion-Induced Aggregation of Conjugated Polyelectrolytes Studied by Fluorescence Correlation Spectroscopy, *J. Phys. Chem. B*, 2013, **117**, 16314–16324.
- 34 F. Zu, F. Yan, Z. Bai, J. Xu, Y. Wang, Y. Huang and X. Zhou, The quenching of the fluorescence of carbon dots: A review on mechanisms and applications, *Microchim. Acta*, 2017, **184**, 1899–1914.
- 35 M. J. O’Connell, E. E. Eibergen and S. K. Doorn, Chiral selectivity in the charge-transfer bleaching of single-walled carbon-nanotube spectra, *Nat. Mater.*, 2005, **4**, 412–418.
- 36 S.-J. Jeon, S.-Y. Kwak, D. Yim, J.-M. Ju and J.-H. Kim, Chemically-Modulated Photoluminescence of Graphene Oxide for Selective Detection of Neurotransmitter by “Turn-On” Response, *J. Am. Chem. Soc.*, 2014, **136**, 10842–10845.
- 37 C. A. Kent, D. Liu, T. J. Meyer and W. Lin, Amplified Luminescence Quenching of Phosphorescent Metal–Organic Frameworks, *J. Am. Chem. Soc.*, 2012, **134**, 3991–3994.
- 38 M. E. Kose, B. A. Harruff, Y. Lin, L. M. Veca, F. Lu and Y.-P. Sun, Efficient Quenching of Photoluminescence from Functionalized Single-Walled Carbon Nanotubes by Nitroaromatic Molecules, *J. Phys. Chem. B*, 2006, **110**, 14032–14034.
- 39 E. T. Niles, J. D. Roehling, H. Yamagata, A. J. Wise, F. C. Spano, A. J. Moulé and J. K. Grey, J-Aggregate Behavior in Poly-3-hexylthiophene Nanofibers, *J. Phys. Chem. Lett.*, 2012, **3**, 259–263.
- 40 F. C. Spano and C. Silva, H- and J-Aggregate Behavior in Polymeric Semiconductors, *Annu. Rev. Phys. Chem.*, 2014, **65**, 477–500.